Rock Mechanics and Rock Engineering
https://doi.org/10.1007/s00603-024-03952-0

ORIGINAL PAPER

Millisecond-resolved gas sorption kinetics and time-dependent diffusivity of coal

Xinxin He[1] · Derek Elsworth[1] · Shimin Liu[1]

Received: 16 January 2024 / Accepted: 1 May 2024

Abstract

We explore the dynamics of gas sorption and diffusion in coal in impacting key mechanisms controlling coal and gas outburst phenomena. We apply a unique time-resolved technique to examine millisecond-resolved gas transport kinetics of CO_2 and CH_4. In particular, we define gas transport response for two distinct coals: one outburst-prone (JH) and the other non-outburst-prone (KINGII). Equilibrium gas sorption and dynamic sorption characteristics are compared between the two coals as proxies for their different outburst responses. Outburst-prone (JH) coal more readily pulverizes during mechanical comminution suggesting ready disintegration compared to non-outburst-prone coals. Sorption capacities of both coals are independent of particle size but influenced by the internal structure and the external geometry of the coal matrix. Cryomilling to reduce particle size enhances gas diffusivity. CH_4-infiltrated coals showed a marked increase in diffusivity with increasing pressure, while CO_2-infiltrated displayed similar trends at higher pressures. A critical finding of the study was the temporal variability in diffusivity. Over time, small time window measurements show that diffusivity decreases with elapsed time, suggesting that only early time-resolved measurements should be used in defining gas outburst potential. Mass fraction methods reveal that early-time diffusion is driven under a steady pressure gradient, shifting later to a transient response—allowing straightforward analysis at early time. This shift is especially significant in understanding outburst-prone coals with complex pore structures. The sorption kinetics analysis confirms that rapid gas transfer predominantly occurs in the early phases of the sorption process when a pseudo-second-order adsorption rate might potentially serve as a predictive index for evaluating the risk of outbursts with the outburst-prone (JH) coal returning a higher rate compared to the non-outburst-prone (KINGII). The findings from this study provide an improved understanding of rapid and dynamic gas transport in the coal matrix with implications for better understanding, characterizing, predicting and mitigating hazardous gas outbursts in coal.

Highlights

- Unique millisecond-resolved technique reveals how different coals react to CO_2 and CH_4 gas sorption, distinguishing between outburst-prone and non-outburst-prone types.
- Gas sorption in coal is influenced by internal structure, not particle size; cryo-milling which mimics the crushing effect during the outburst enhances gas diffusion.
- Early-time gas diffusion measurements are crucial; they decrease over time, highlighting the importance of early-time gas diffusion measurements in coal and providing key insights into outburst risks in coal mines.
- Kinetic sorption analysis shows fast gas transfer in early sorption stages, with a higher pseudo-second-order adsorption rate in outburst-prone coal, suggesting a potential risk indicator.

Keywords Coal gas outbursts · Gas sorption · Diffusivity · Time-resolved analysis · Coal pulverization · Sorption kinetics

✉ Shimin Liu
szl3@psu.edu

[1] Department of Energy and Mineral Engineering, G3 Center and EMS Energy Institute, The Pennsylvania State University, University Park, PA 16802, USA

Published online: 20 May 2024

Abbreviations

n_a	Adsorbed gas at equilibrium, mol
n_t	Total gas injected, mol
n_f	Free phase gas, mol
$n^t_{a,i}$	Adsorbed gas at time t during step i, mol
$n^1_{ref,}$	Total gas injected during step i, mol
n^t_{ref}	Gas in the reference cell as the free phase at time t during step i, mol
n^t_{samp}	Gas in the sample cell as the free phase at time t during step i, mol
n^0_{samp}	Gas in the sample cell as a free phase during step i before injection, mol
V_a	Volume of gas adsorbed, mL
V_{ref}	Volume of the reference cell, mL
V_{void}	Volume of the void space, mL
T_{STP}	Temperature at standard conditions, 273.15 K
p_{STP}	Pressure at standard conditions, 14.6959488 psi
t_{oil}	Temperature of oil bath, 35 ℃
$V^{STP}_{t,i}$	Volume of gas injected at step *i* in standard conditions of temperature and pressure, mL
$p^0_{ref,i}$	Pressure in the reference cell before gas injection at step *i*, psi
$Z^0_{ref,i}$	Compressibility factor in the reference cell before gas injection at step *i*
$p^1_{ref,i}$	Pressure in the reference cell after gas injection at step *i*, psi
$Z^1_{ref,i}$	Compressibility factor in the reference cell after gas injection at step *i*
$p^{eq}_{f,i}$	Pressure at equilibrium for step *i*, psi
$Z^{eq}_{f,i}$	Compressibility factor at equilibrium for step *i*
$V^{STP}_{a,i}$	Volume of gas adsorbed at step *i* in standard conditions of temperature and pressure, mL
$V_{m,g}$	Molar volume of gas in free phase, mL/mol
$V^{STP(ex)}_{a,i}$	GSE at step *i* in standard conditions of temperature and pressure, mL
ρ_g	Density of gas in free phase, mL/g
ρ_a	Density of gas in adsorbed phase, mL/g
V_a	Volume of gas adsorbed, mL
P	Adsorption pressure, psi
V_L	Langmuir volume, m^3/t
P_L	Langmuir pressure, psi
C	Surface concentration, g/g
r	Radius of the coal particles, m

1 Introduction

Coal and/or coal–gas outbursts are sudden and violent coal failures associated with abrupt gas release from a stressed coal formation typically triggered by perturbations of stress and/or gas pressure as buttressing confinement are removed. The hazardous and unpredictable nature of coal outbursts makes them a considerable threat to underground coal miners, complicating efforts to control and mitigate their dangers. Therefore, mechanism-based investigation of these outbursts is crucial for sustainable extraction of these natural resources in the next few decades.

According to the most recent International Energy Agency (IEA) report (2023) (International Energy Agency 2023), global coal consumption reached an all-time high in 2022 because of the economic recovery following the COVID-19 pandemic. Even though the necessity of transitioning away from coal has been discussed for achieving the climate goals, it will be a slow and steady process toward the final energy transition. Coal plays a complex and intricate role in the context of the United Nations Sustainable Development Goals (SDGs) (United Nations 2015; Arora and Mishra 2019). Coal mining has economic impact in development (SDG 8—Decent work and Economic Growth) in coal producing regions, such as Appalachian Basin (PA, WV, VA, AL, and KY) and Illinois Basin (IN, IL, and KY). Mining is a significant economic activity providing jobs and contributing to local economies. Coal can also impact energy access and affordability (SDG 7—Affordable and Clean Energy). Coal has historically been a major source of energy contributing to energy security and enabling industrialization. Thus, the coal mining industry should have a proactive vision for future sustainable development by treating coal as a part of solution rather than a problem. Specifically, sustainable coal mining needs to continue to address the safe mining conditions (SDG 3—Good Health and Well-being). There is a need to address the outburst-induced mine safety and health hazards to reduce accident risks and ensuring operational continuity for cleaner production.

Characteristic of such outbursts is the concurrent and rapid release of liberated gas with significant expansion energy and with CH_4 and CO_2 comprising the most common source gasses (Beamish and Crosdale 1998). Historical records indicate that coal–gas outbursts were reported as early as the eighteenth century in various mining regions (Lama 1996). Our understanding of coal outbursts has evolved and improved over time, but some fundamental mechanisms remain unclear due to the complexity of the multi-physical processes and interactions involved during coal failure. Dating back a century ago, these events were even attributed to supernatural causes and considered unpreventable. However, as coal mining advanced and safety practices improved, significant engineering success followed in mitigating and reducing the unexpected occurrence of outbursts. In particular, the widespread adoption of inducer short-firing following Lange's work (Lange 1892) spurred coal operators and researchers to investigate geological and

geotechnical factors contributing to this dynamic phenomenon. During the twentieth century, coal outbursts received increased attention from researchers and regulatory agencies with the rapidly increasing need for coal as an energy source. A "Committee for Research on Outbursts" was first formed in France in 1913 and similar organizations followed in different countries where many of them continue to operate until today. Scientific studies began to explore the underlying mechanisms and factors contributing to coal–gas outbursts. Such studies first involved the statistical analysis of the features of where the outbursts occurred and the progression of events during the outbursts, identifying that: outbursts tend to occur more frequently with increasing mining depth in associated with certain geological structures (Hargraves 1983; Qixiang 1990); outbursts occur mostly during the initial entry development in coal seams with perturbations of drilling, cutting, and blasting (Lama 1996; Cao et al. 2016); burst precursors include elevated audible sound levels, excessive coal spalling, temperature variation, drill rod clogging, noticeable bumps, excessive gas-outing, abrupt seismic events, among many other signals.

In addition to statistical analysis, hypotheses were advanced to explain why outbursts occur, including that outbursts are: triggered by stress and gas with one potentially more influential than the other in specific instances (Hanes et al. 1983). A consequence of the instability in coastal/rock structures caused by varying gas pressure gradients (Paterson 1986), triggered by earthquakes(Sato and Fujii 1989). A catastrophic event propelled by energy released from gas desorption (Hou et al. 2021) and for which measuring the initial expansion energy of the released gas provides a method for outburst prediction. However, given the complexity of the dynamic process, these hypotheses provide only partial explanations to understanding the phenomenon. However, summarizing all major contemporary hypotheses suggests a consensus that the outburst process can be divided into four stages: preparation, triggering, development, and termination, as shown in Fig. 1. Within these four stages, gas plays a key role in the development stage both in crushing and transporting the coals. Indeed, the work involved in comminution in an outburst could be 13.96 times greater than that involved in the ejection/transport of the coal(Tu et al. 2021). This indicates that the coal has been crushed and pulverized before and during the process of being ejected into the working void space. Post-outburst statistical analysis of the coal itself also reveals a common particle size distribution (PSD) property of the outburst coal (Jin et al. 2018; Tu et al. 2021). In most of these distributions, a single peak with a broad distribution is observed. Thus, using a single particle diameter to estimate gas diffusion behavior remains somewhat questionable. Thus, in this study, powdered coal samples from the same coal were prepared in two particle sizes to evaluate their sorption and diffusion properties with size—and in particular their diffusivity.

The roles of coal properties, gas content, stress distribution, and geological structure in contributing and modulating outbursts have also been broadly investigated. Gas content/pressure is an expected prerequisite in understanding the triggering and development mechanisms of the outburst due to the rapid discharge of gas during the very initial stage of the outburst—as this is when the massive expansion of gas and its energy release is observed within the first 10 s if triggering (Jiang et al. 1996; Valliappan and Wohua 1999; Wang et al. 2019). Congruent with this observation, many indexes derived from gas content/pressure have been developed as an indicator of outburst-risk. These include Ettinger's sorption/desorption index, K_T index and the Δp express index (Lama 1996). However they all average gas sorption or discharge properties over an extended period of time, with only the Δp express index capturing gas pressure changes in the first 10–60 s. Ignorance of the dynamics of gas release and transport at early time may fail to define the overall dynamic energy release potential of the sorbed and/or compressed (free) gas. As a part of coal–gas outburst prevention, burst

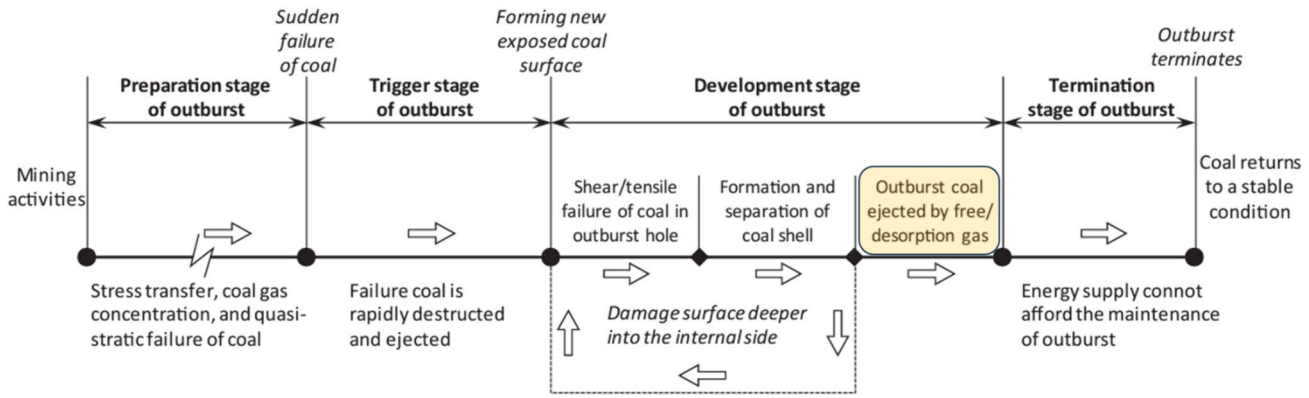

Fig. 1 Four stages in the dynamic process of an outburst (Jin et al. 2018)

precursors have been developed and monitored at field sites and include micro-seismic monitoring (Zhenbi and Baiting 2012; Si et al. 2015; Ding et al. 2016) and real-time gas monitoring (Nie et al. 2014; Zhang et al. 2022; Wang et al. 2021), among others. For mitigation and prevention, various strategies to mitigate the risk of coal outbursts have been proposed and include: gas drainage to decrease gas content; stress management to eliminate triggering and initiation; mine layout optimization to minimize abutment pressures, and; panel-wide cutting sequence optimization to control stress distributions, together with others. Even though significant progress has been made toward elimination of the hazard, the cramped and difficult field conditions and the limitations in data processing capacity underground, render most in situ monitoring systems capable of providing useful information for post-outburst investigations. Other than the time-averaged index and the limitations of being unable to capture the outburst initiation time window, a time-resolved method applied to the initiation of the outbursts is necessary to reveal how outbursts initiate and build. To this goal, we measure pressure changes at a temporal resolution to 0.1 ms following gas sorption (when considering physisorption from a physics perspective, adsorption and desorption processes are often treated as equivalent).

The initiation of an outburst begins with excessive gas desorption serving as the energy source for either fragmenting the coal by creating new surfaces for energy dissipation. This is central to dynamically displacing, spalling, and/or shattering coal toward free space—in reality both comminution and transport occur near-simultaneously during burst incidents. Different from most conventional gas reservoirs, coal is a typical organic source rock that both generates (igneous intrusions for CO_2) and traps CH_4 within the coal itself (Moore 2012), where 90–98% of the CH_4 or CO_2 is stored in an adsorbed state (Gray 1987; MENG et al. 2014). Three key gas migration processes operate in coal seams, viz.: i) adsorption/desorption; ii) diffusion; and iii) Darcian transport. Among all three processes, adsorption/desorption serves as the sink and source for gas transfer, with the molecular interaction with the coal is believed to be functionally instantaneous. Transport occurs with free gas in the form of Darcian flow within the cleat and fracture networks. Diffusion controls the gas migration from the source in the coal matrix to the fracture and thus is a deterministic process to understand how gas is discharged in any given outburst event. The systematic study of coal diffusivity began in the mid-twentieth century when it was apparent that the diffusion of gasses, such as CH_4, CO_2, and N_2, through coal seams significantly impacted mine safety (Lama 1996). Understanding coal diffusivity was crucial in developing effective gas drainage techniques to reduce the risk of gas outbursts and explosions. Experimental techniques have been developed to measure coal diffusivity under various conditions, for different gasses and varying coal samples in size, rank, moisture content, and subject various pre-treatment techniques (Yang and Liu 2020a)—to understand how factors, such as pressure, temperature, and coal properties influenced diffusivity. Theoretical models have also been developed to describe the diffusive behavior of gases in coal. Based on Fick's second law, unipore, bidisperse, and time-dependent diffusion models have all been proposed to define gas diffusive behavior. Other models also consider the porous nature of coal including its microstructural features, such as tortuosity, fractal dimension (Yang and Liu 2021), and direct interactions, between gas molecules and coal surfaces.

These models have significantly improved our understanding of gas transport within the coal matrix; however, all these models rely on long-term (minutes to hours) measurements involving mass equilibration estimate gas diffusivity. These necessarily long-term methods,neglect the early-time dynamic aspects of gas transport by both neglecting ultra-early-time measurements and in fitting over a large time interval, which may result in the incorrect characterization of gas transport behavior in the short-term. This may subsequently affect the fidelity of gas burst predictions since the peak gas transport response is missed. In the following, we address this early-response deficiency by measuring early desorption response at (0.1) millisecond resolution. We record these measurements on contrasting outburst-prone and non-outburst-prone coals prepared to represent a spectrum of (two) different size distributions for sorption and diffusion measurements to capture the dynamics of early-time gas transport. This study provides a first-of-its-kind millisecond-resolution characterization and data recovery and analysis to establish the early-time dynamics of gas storage and sorption.

2 Experimental work

2.1 Sample collection and preparation

The coal samples were sourced from two distinct locations: the King Coal II Mine (samples later denoted as KINGII) located in the San Juan Basin of Colorado, USA, and the Jinhe Coal Mine (later denoted as JH) located in the Minghe Basin in Gansu, China. Both are sourced from underground coal mines with the Jinhe Coal Mine identified as burst-prone and the King Coal II Mine non-burst-prone. Moreover, the samples obtained from the burst-prone Jinhe Coal Mine were specifically gathered from areas that have undergone tectonic deformation—typically fracturing the coal and lowering the permeability. The rationale behind selecting these two varieties of coal for comparative analysis lies in the desire to probe fundamental differences in their

time-resolved diffusivity during the initial stages of mass transfer—as a proxy for burst-proneness. Such an examination has never previously been investigated nor reported. The insights gained from this comparison will be valuable in understanding the controls of gas transport behaviors in distinguishing burst-proneness.

Samples were collected from active mining faces, sealed immediately within sample buckets, and transported to the laboratory for further analysis. Sample preparation starts with hand-crushing in a steel mortar to shield the coal from thermo-alteration with the crushed powders sieved to 60–80 mesh and preserved for subsequent experiments. This particle size range is consistent with that recommended for isotherm measurements as suggested by Mavor et al. (Mavor and Pratt 1990). Moreover, by grinding the coal to 60–80 mesh, we ensure that gas transport occurs solely through diffusion within the coal matrix, effectively eliminating the influence of mass transfer in cleats via Darcian flow (Yang 2019; Yang and Liu 2019; Liu et al. 2020b, a). As shown in Fig. 2, the coning and quartering method was used to separate the coal particles into replicate sub-samples, according to the ASTM standard (ASTM International 2018). One of these sub-samples was immediately placed into the sorption measurement system after being oven-dried at 90 °C for 12 h, ready for the adsorption and diffusion test. Many previous studies (Nandi and Walker 1969; Nikolai Siemons et al. 2003a; Cui et al. 2004) have indicated that diffusion measurements are insensitive to size when the particle size exceeds 0.1 mm. To assess the impact of matrix breakage, and thus size reduction, on diffusion, another duplicate sub-sample was subjected to further cryogenic grinding (Mixer mill mm 400, Germany). This was followed by another oven-drying at 90 °C for 12 h, before being used for the same sorption testing. The cryogenic grinding process is protected by liquid nitrogen from generating excess heat and damaging the coal samples. Before the cryogenic grinding, the sample is vacuum-dried to remove free water, preventing possible alteration of the pore structure due to ice formation at low temperatures. It is also important to note that during the cryogenic grinding process, there is no direct contact between the liquid nitrogen and the sample powder in the milling cell. These precautions ensure that any changes in pore structure are primarily due to mechanical matrix breakage, not the cryogenic process itself. Meanwhile, the cryogenic treatment may influence the fracture system but not down to the pore system(Yang and Liu 2020a; Qin et al. 2022; Hou et al. 2022; Huang et al. 2023); however, due to the extensive milling in this paper, the fracture system is already destroyed. Therefore, no structural changes occur due to the cryogenic treatment. The grinding is set for 2 min and 5 cycles for all samples to ensure the same degree of grinding. Before and after the cryogenic grinding, particle size distribution was measured for the samples using a Laser Diffraction Particle Size Analyzer (Mastersizer 3000, USA) with a window measuring particle sizes from 10 nm to 3.5 mm. Using the cryogenic grinding, the coal particle sizes can be reduced significantly to micro- through nano-meter scale for intercomparison.

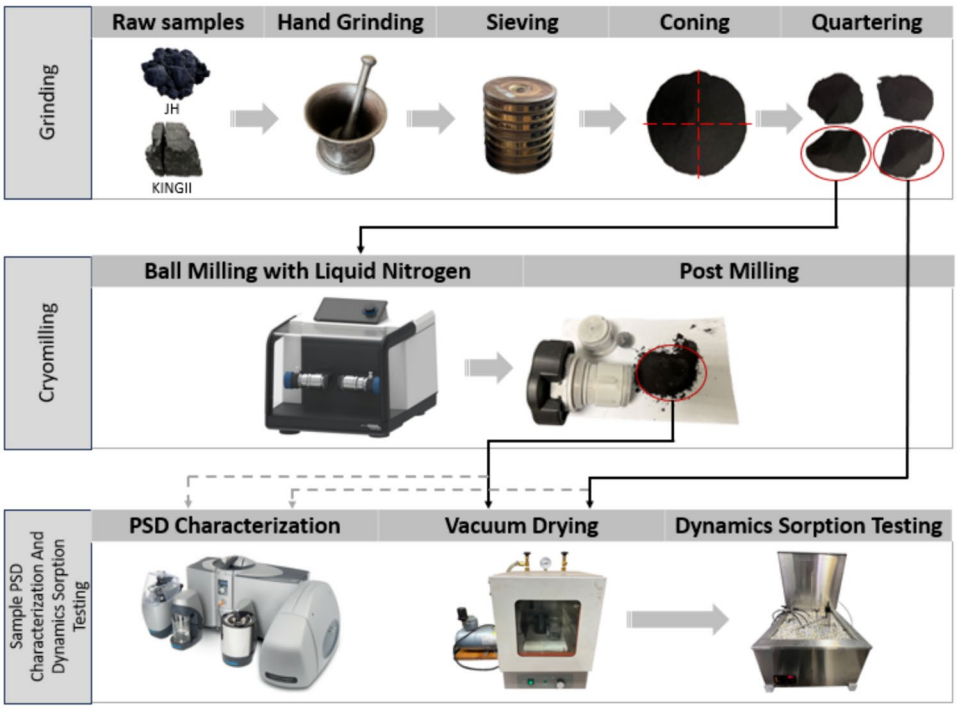

Fig. 2 Sample preparation procedures

2.2 Experimental setup and procedures

Various sorption measurement methods can be categorized among volumetric, manometric, and gravimetric methods (He et al. 2020). Within the coal outburst and coalbed methane (CBM) research community, the manometric method is widely adopted for its reliability and scalability (Liu et al. 2020b; Yang and Liu 2020b). We apply millisecond-resolution pressure transducers to capture very-early-time pressure data. Our newly established sorption measurement system has the ability to discern time-resolved pressure change during the diffusion process. A schematic of the system is shown in Fig. 3(a). The system comprises two sorption units each with a pressure capacity of 3000 psi (20.7 MPa). These are submerged in a thermostat-controlled water/anti-freeze bath capable of maintaining a steady temperature between -20 and 150 °C with a precision of ± 0.1 °C. Additionally, the setup features a vacuum pump and pressure transducers, coupled with a data acquisition system capable of sampling at a rapid rate of 0.1 ms. The integrated pressure transducers in the system have an accuracy of ± 0.04% of full scale and function effectively over the temperature range -20 to 80 °C.

For each testing unit, ~ 25 g of each dried sample was loaded into the sample cells. Before any sorption measurement, both samples were degassed to 1 psi (0.03 MPa) for 10 min to remove extraneous gas and moisture contamination from the air during the transfer from the vacuum oven to the sorption system. The water bath thermostat was then set to 35 °C to begin the measurement of void volume of the samples using helium expansion (helium purity > 99.999%)—using four measurements with the closest three values averaged. Sorption measurements were initiated immediately after completion of the void space measurement. CH_4 or CO_2 was first injected into the reference cell to a prescribed pressure and when the pressure stabilized the valve between the reference cell and the sample cell was opened to allow the start of adsorption. During this process the data acquisition system sampled at a frequency of 10 K Hz (0.1 ms per data recording) for 20 min then switched to 1 Hz (1 s) until the pressure remained constant—typically over one hour. This represented a single data point describing the isotherm. Two recording windows are shown in Fig. 3b as the initial sorption process and sorption at equilibrium. The first window is used to define the (short-term) diffusion profile and the second the (long-term) sorption properties. As depicted in Fig. 3b, this sequence was repeated six times at incremented pressures, continuing through final pressure equilibrium—defining the full isotherm. For this study, the targeted equilibrium pressures were set at 150, 300, 500, 700, 1000, and 1300 psi (1.03, 2.07, 3.45, 4.83, 6.89, and 8.96 MPa) for methane (CH_4) which covers a typical in situ pressure range for coal seams and 200, 300, 400, 550, 750, and 800 psi (1.38, 2.07, 2.76, 3.79, 5.17, and 5.52 MPa) for carbon dioxide (CO_2) to prevent the phase chang and the formation of supercritical fluid.

2.3 Gas sorption capacity

The resulting raw data yield Gibbs surface excess (GSE) capacities by assuming a constant void space and relating sorption space to a surface with no thickness (Lowell et al. 2006; Rouquerol et al. 2013). To convert the GSE to absolute adsorbed mass, the adsorbed mass of gas at any pressure may be calculated as:

$$n_a = n_t - n_f \tag{1}$$

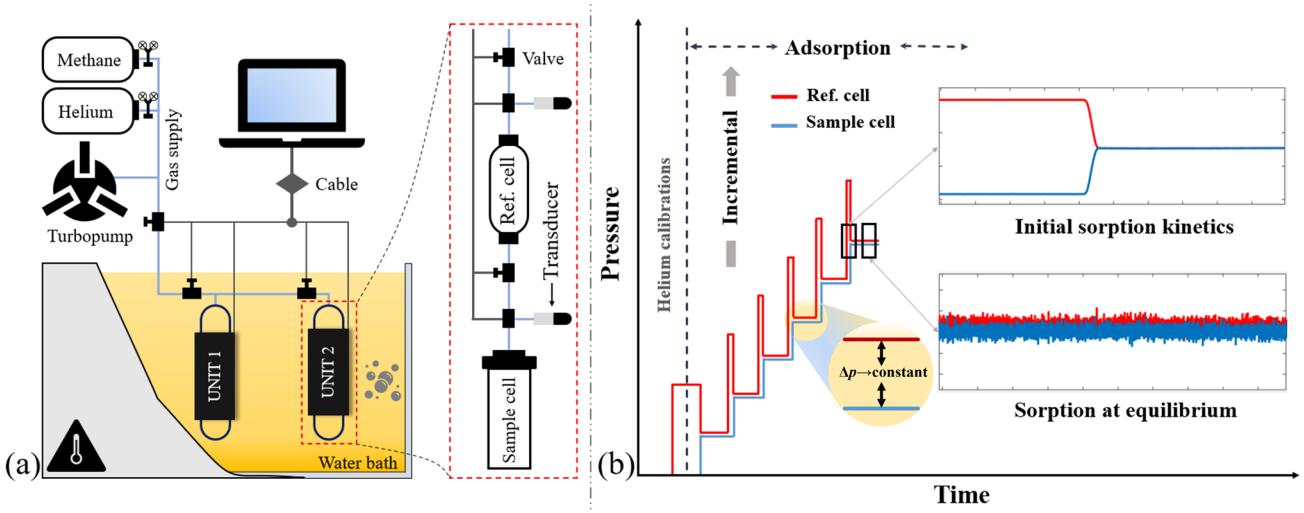

Fig. 3 **a** Sorption kinetics measurement system; **b** Experimental procedure

Equation (1) may be converted to volumetric form through the real gas equation of state (EOS) $pV = ZnRT$. Then the volume of gas injected into the reference cell at step i, corrected to standard conditions of temperature and pressure (STP), is determined as:

$$V_{t,i}^{STP} = \sum_{i=1}^{n} \left(\frac{p_{ref,i}^{1}}{Z_{ref,i}^{1}} - \frac{p_{ref,i}^{0}}{Z_{ref,i}^{0}} \right) \frac{T_{STP}}{(T_{STP} + t_{oil}) p_{STP}} \tag{2}$$

The volume of the reference cell and the void space in the sample cell constitute the free space in each cell, so the gas occupying the free space at each step is determined as:

$$V_{f,i}^{STP} = \left(\frac{p_{f,i}^{eq}}{Z_{f,i}^{eq}} \right) \frac{T_{STP}(V_{ref} + V_{void})}{(T_{STP} + t_{oil}) p_{STP}} \tag{3}$$

Combining Eq. (1)–(3) results in:

$$V_{a,i}^{STP} = \left\{ \sum_{i=1}^{n} \left(\frac{p_{ref,i}^{1}}{Z_{ref,i}^{1}} - \frac{p_{ref,i}^{0}}{Z_{ref,i}^{0}} \right) V_{ref} - \left(\frac{p_{f,i}^{eq}}{Z_{f,i}^{eq}} \right) (V_{ref} + V_{void}) \right\} \frac{T_{STP}}{(T_{STP} + t_{oil}) p_{STP}} \tag{4}$$

However, the void space, V_{viod}, in Eq. (4) reduces during the experiment as the gas pressure increases as a multilayer adsorption film forms of increasing thickness. Thus, some corrections are needed to Eq. (1), as:

$$n_a = n_t - \frac{(V_{ref} + V_{void}) - V_a}{V_{m,g}} \tag{5}$$

By simplifying and reorganizing Eq. (5), we obtain:

$$n_a - \frac{V_a}{V_{m,g}} = n_t - \frac{(V_{ref} + V_{void})}{V_{m,g}} \tag{6}$$

where V_a denotes the absolute adsorbed amount. It is clear that the right side of Eq. (6) conforms to the definition of the GSE and $\frac{(V_{ref} + V_{void})}{V_{m,g}} = n_f$. By substituting Eq. (4) with $V_{a,i}^{STP(\text{ex})}$ and V_a in Eq. (6) with $V_{a,i}^{STP}$, the following is obtained:

$$V_{a,i}^{STP} = \left(V_{a,i}^{STP(\text{ex})} - n_a \right) V_{m,g} \tag{7}$$

Then, combined with the physical properties of the gas, Eq. (4) is corrected as:

$$V_{a,i}^{STP} = \frac{\left\{ \sum_{i=1}^{n} \left(\frac{p_{ref,i}^{1}}{Z_{ref,i}^{1}} - \frac{p_{ref,i}^{0}}{Z_{ref,i}^{0}} \right) V_{ref} - \left(\frac{p_{f,i}^{eq}}{Z_{f,i}^{eq}} \right) (V_{ref} + V_{void}) \right\} \frac{T_{STP}}{(T_{STP} + t_{oil}) p_{STP}}}{1 - \frac{\rho_g}{\rho_a}} \tag{8}$$

The NIST Standard Reference Database 69 (Linstrom and Mallard 2001) was used to determine compressibility factor (Z) and density (ρ) used in this study.

We model the CH_4/CO_2-Coal-gas sorption isotherms by the Langmuir equation because of its simplicity and wide acceptance for describing coal gas sorption isotherms (Hu et al. 2020; Yang et al. 2022). The Langmuir equation with two parameters is defined as:

$$V_a = \frac{V_L p}{P_L + p} \tag{9}$$

2.4 Real-time sorption dynamics

We also desire to capture the short-time desorption dynamics to supplement the equilibrium sorption capacity. Since pressures are continuously monitored and recorded following each pressure-increment, conservation of mass (as described in Eq. (1)) may be used to determine gas adsorption in real time as:

$$n_{a,i}^{t} = (n_{ref,i}^{1} - n_{ref,i}^{t}) - (n_{samp,i}^{t} - n_{samp,i}^{0}) \tag{10}$$

Substituting the monitored pressures, yields:

$$n_{a,i}^{t} = \left[\left(\frac{p_{ref,i}^{1}}{Z_{ref,i}^{1}} - \frac{p_{ref,i}^{t}}{Z_{ref,i}^{t}} \right) V_{ref} - \left(\frac{p_{samp,i}^{t}}{Z_{samp,i}^{t}} - \frac{p_{f,i-1}^{eq}}{Z_{f,i-1}^{eq}} \right) V_{void} \right] \frac{1}{R(T + t_{oil})} \tag{11}$$

Finally, the sorption dynamics can be expressed in the form of sorption fraction to time as:

$$\frac{M_t}{M_\infty} = \frac{n_{a,i}^{t}}{n_{a,i}} = \left[\left(\frac{p_{ref,i}^{1}}{Z_{ref,i}^{1}} - \frac{p_{ref,i}^{t}}{Z_{ref,i}^{t}} \right) V_{ref} - \left(\frac{p_{samp,i}^{t}}{Z_{samp,i}^{t}} - \frac{p_{f,i-1}^{eq}}{Z_{f,i-1}^{eq}} \right) V_{void} \right] \frac{1}{V_{a,i} R(T + t_{oil})} \tag{12}$$

where the $n_{a,i}$ is the mass of gas adsorbed within a selected time window.

2.5 Gas diffusivity

Gas diffusion may be defined in terms of Fick's second law of diffusion, as:

$$\frac{\partial C}{\partial t} = \left(D \frac{\partial^2 C}{\partial x^2} + D \frac{\partial^2 C}{\partial y^2} + D \frac{\partial^2 C}{\partial z^2} \right) \tag{13}$$

assuming that the diffusion coefficient is constant in both space and time. For our experimental system we assume that the coal particles are spherical and that diffusion is restricted to radical flow. Then, Eq. (13) can be restated in spherical coordinates as:

$$\frac{\partial C}{\partial t} = D \left(\frac{\partial^2 C}{\partial r^2} + \frac{2 \partial c}{r \partial r} \right) \tag{14}$$

Furthermore, if we assume that the surface concentration of the gas (r = a) C_0 is constant and the sphere has an initial uniform concentration C_1, the solution of Eq. (14) is expressed as an infinite series as:

$$\frac{C - C_1}{C_0 - C_1} = 1 + \frac{2a}{\pi r} \sum_{n=1}^{\infty} \frac{(-1)^n}{n} \sin \frac{n\pi r}{a} e^{(-Dn^2\pi^2 t/a^2)} \tag{15}$$

We can rewrite Eq. (15) in the form of the total mass of gas entering or leaving the sphere, Eq. (15) takes the form of

$$\frac{M_t}{M_\infty} = 1 - \frac{6}{\pi^2} \sum_{n=1}^{\infty} \frac{1}{n^2} e^{(-Dn^2\pi^2 t/r^2)}$$

$$D_e = \frac{D}{r^2} \tag{16}$$

where D_e is the effective diffusivity. Effective diffusivity (later referred to as diffusivity) is used in this study, as it normalizes for differing particle sizes among samples.

2.6 Data processing for time-resolved diffusion process

The recorded pressures during the 20-min fast data logging period were both voluminous and noisy—requiring extensive pre-processing. The flowchart in Fig. 4 shows the completed procedure for data processing to estimate the final time-resolved diffusivity. Initially, as depicted in Fig. 4b, the noise was filtered using a trailing moving average (TMA), assuming that the noise is randomly distributed around the actual mean value; then following the filtering, the very-large data set was decimated with the proviso that adjacent points retained a minimum overlap with the TMA process. Contrasting Fig. 4a, b demonstrate that this process managed the noise while preserving the essential information of the data set. Ideally, at pressure equilibrium, the pressure response in the testing cells should monotonically decrease, as the gas diffuses into the coal matrix under isothermal conditions. However, in reality, the operation of the valve introduces an abrupt temperature change and mechanical pulse in each of the cells due to the rapid gas compression from the reference to the sample cell. This thermodynamic step causes the pressure to be unsteady and chaotic. To address this matter, a Cubic Spline Interpolation (CSI) was first employed to smooth the pressure data. This method effectively reduced oscillations between data points while retaining critical information, as illustrated in Fig. 4d and (d.1). Following CSI application, we established a criterion to identify the last maximum pressure point as the starting point for our diffusion analysis. This approach is based on the assumption that the pressure drop is primarily governed by mass transfer following the last maximum pressure point. Furthermore, as shown in Fig. 4f, (f.1), and (f.2) to maintain local monotonicity, a higher-order polynomial curve fitting was applied to the CSI-processed data to complete the data pre-processing. This strategy helps eliminate Runge's phenomenon, known to cause extreme oscillations in high-degree polynomial interpolations. The pre-processed data were then used to determine dynamic time history of gas sorption through time-resolved diffusivity calculations according to the diffusion equation. Data pre-processing was completed in MATLAB as illustrated in Fig. 4.

3 Results and Discussion

3.1 Particle size characterization and distributions

We use a Mastersizer 3000 laser diffraction particle analyzer to measure particle size, requiring careful control of the sample concentration. This concentration must be sufficient concentrated to allow the laser to produce diffraction at a certain ideal intensity but sufficiently dilute to prevent obscuring the signal. Therefore, in a laser diffraction system, the concentration of the sample is indicated by a parameter known as laser obscuration, defined as the percentage reduction in light intensity as the beam passes through the sample. It is crucial to maintain consistent laser obscuration levels across similar measurements to ensure the comparability of their results. Table 1 displays that the laser obscuration levels for both hand pulverized and cryomilled samples remain under the established threshold of 15% (see also supplemental material in Table S-1). Additionally, the values are notably similar within each specific milling condition. This consistency supports the validity of the results and facilitates comparisons among samples.

One direct observation from the size distribution profile in Fig. 5 shows that the original 60–80 Mesh samples for JH and KINGII were both distributed over a range larger than the sieve sizes used to screen them. This suggests that neither of the samples forms perfect spheres. When analyzed on a linear scale (Fig. 5) it is observed that the JH sample exhibits greater asymmetry relative to the mode diameter and possesses a larger proportion of particles exceeding 60 mesh in size compared to KINGII. This implies that JH has a more pronounced elongated axis, resembling an ellipsoid. This characteristic could be attributed to JH undergoing extensive tectonic deformation and stressing to yield this structure. Under identical cryo-milling conditions, the prepared samples shows a dramatic difference between JH and KINGII samples. As shown on the left side of Fig. 5, although a notable portion of particle size ranging from 1 to 100 µm has been generated for both of the samples, it is clear that the pulverized JH sample is much smaller compared to KINGII under the same milling procedures. A *span = (D90—D10)/*

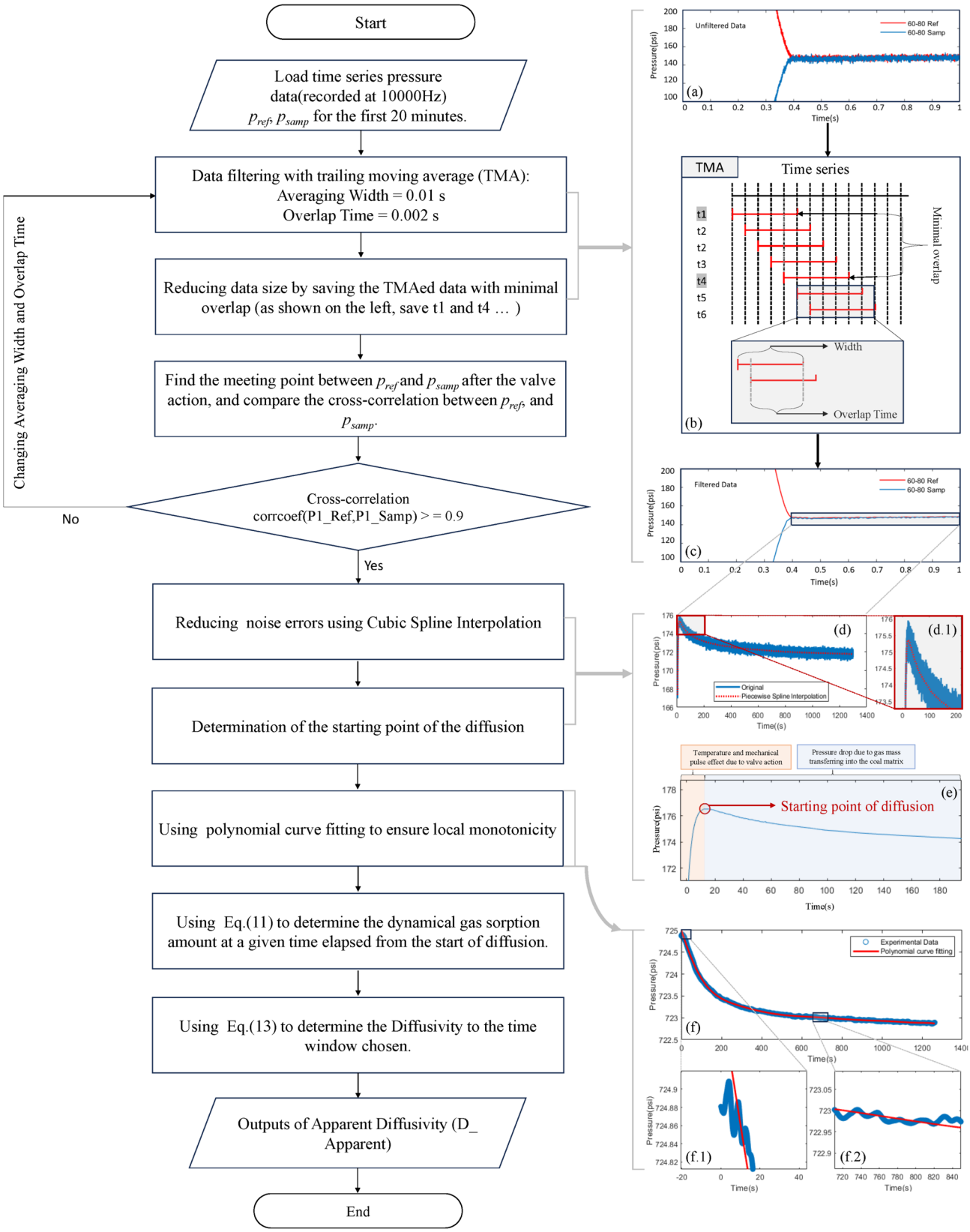

Fig. 4 Flowchart of data processing procedure for estimating time-resolved diffusivity

Table 1 Laser diffraction particle size analysis and adsorption capacity modeling results

Sample	Laser Diffraction Particle Size Analysis			Sorption Capacity Modeling		
	Laser Obscuration (%)	Span (1)	SSA (m^2/kg)	Gas	Langmuir Volume (cc/g)	Langmuir Pressure (psi)
KINGII 60–80 Mesh	8.8	0.7	28.4	CH_4	24.0	372.7
				CO_2	63.9	461.2
JH 60–80 Mesh	8.5	0.7	24.4	CH_4	27.2	403.1
				CO_2	88.4	517.0
KINGII Cryomilled	12.9	1.7	169.5	CH_4	24.4 (↑)	361.2
				CO_2	67.9 (↑)	431.9
JH Cryomilled	10.9	5.6	1188.0	CH_4	25.5 (↓)	355.4
				CO_2	97.2 (↑)	641.0

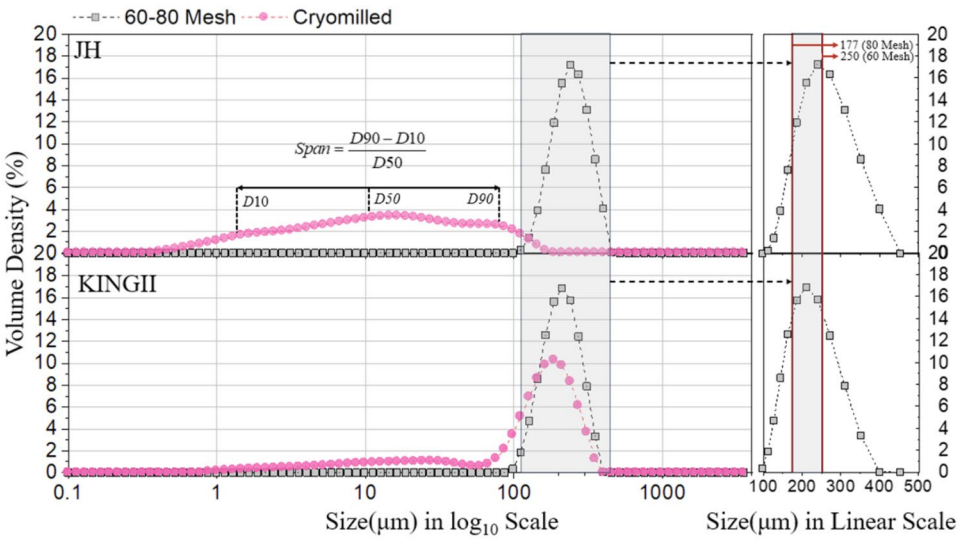

Fig. 5 Size distribution both before then after cryogenic milling

D50 characterizes how the 10% and 90% distributions contrast when normalized against the midpoint—where *D10, D50* and *D90* define the diameters of the particle size distribution curve corresponding to 10%, 50% and 90% finer as illustrated in Fig. 5.

Referring to Table 1, the span of KINGII expanded by a factor of 2.26, whereas JH the increase was more significant, at 7.53 times. This size reduction significantly increases the external specific surface area (e-SSA) measured by laser diffraction. For unmilled samples, the external surface areas are almost identical for both JH and KINGII samples. After cryomilling, the external surface area for JH is approximately one order of magnitude larger than KINGII, due to the small sample size of the JH sample as illustrated in Fig. 5. JH is an outburst-prone coal and the cryo-milling induced significant size reduction—maybe as a result of weak inter-particle cohesive force. In other words, the JH coal can be easily pulverized due to the low particle–particle interaction strengths. This feature determines its easiness of breaking under any given dynamic trigger events, including over stressing, excessive and abrupt gas desorption, mining induced tremor and others.

3.2 Sorption properties

Equilibrium sorption is estimated according to the method described in Sect. 2. The sorption profiles of the four samples tested with CH_4 and CO_2 are shown in Fig. 6. Within the pressure range tested for both CH_4 and CO_2, the mass adsorbed on JH slightly decreased for the cryomilled coal compared to the coarser fraction (60–80 mesh). Conversely, adsorption increases for KINGII following cryomilling. These results are consistent with prior observations indicating that particle size does not have a definitive impact on coal sorption capacity (Zhao et al. 2021). This is consistent with the supposition that size reduction does not impact coal

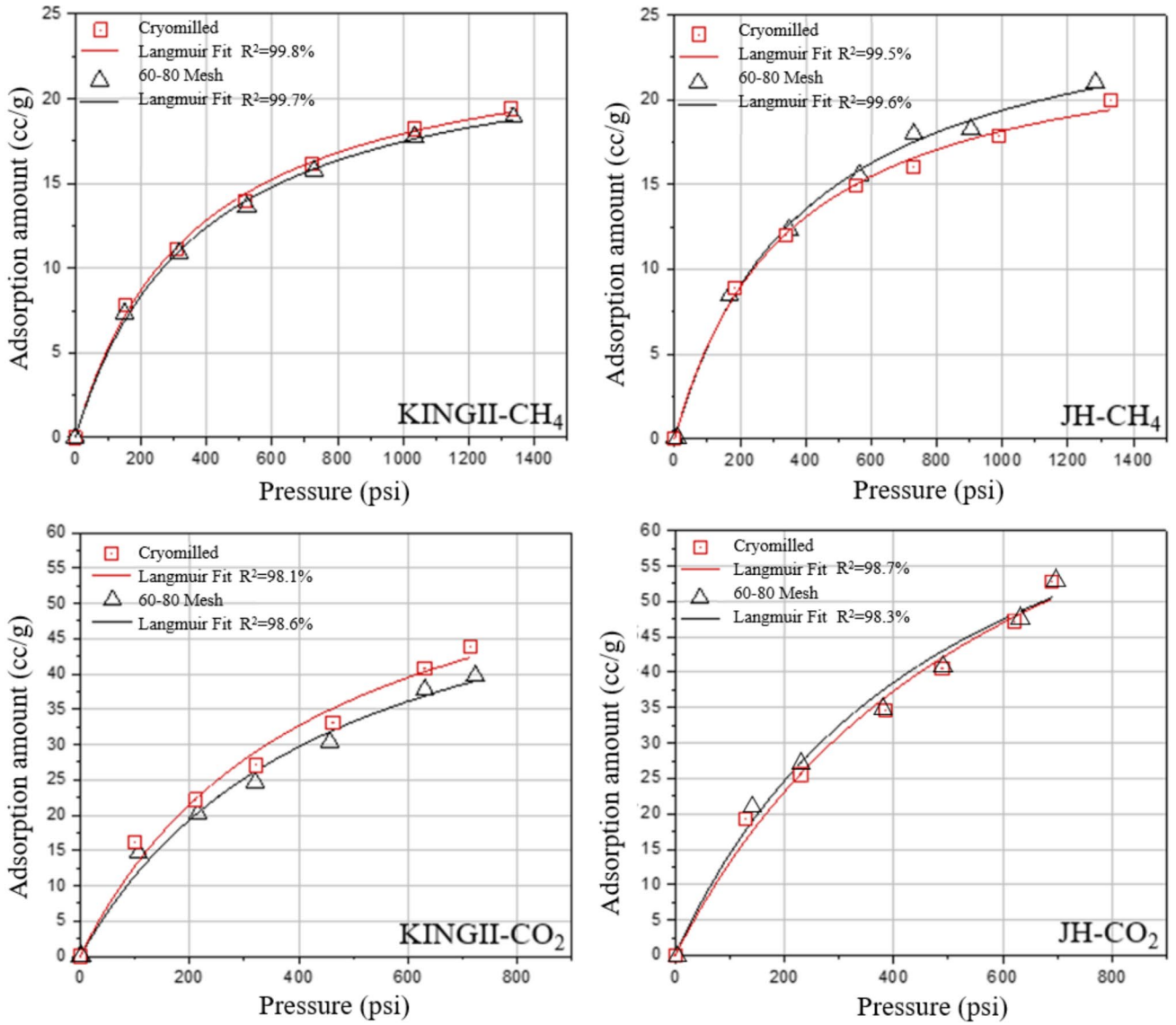

Fig. 6 Sorption capacity of CH_4 and CO_2 on raw and cryomilled coal samples

porosity (Ruppel et al. 1974) and only impacts particle size (Guo et al. 2014). Variations in ash and maceral composition of the different grain size fractions are also explained as causes of the inconclusive impact of particle size on sorption capacity (Busch et al. 2004). Thus, variation in size cannot be the dominant effect for gas sorption determination as stated in some other reported work. Additionally, the intrinsic properties of micropore volume (Hu et al. 2020) and/or composition changes should be considered for the ultimate sorption capacity prediction.

The Langmuir model was employed for the sorption data modeling. The results are shown in Fig. 6 and Table 1, where the fit closely matches the experimental data points. Despite the Langmuir model representing monolayer sorption, which differs from contemporary multilayer sorption theories, it remains highly effective and is widely utilized (Ruppel et al. 1974; Yang 2020; He et al. 2020; Yang et al. 2022). The effect of milling on the ultimate sorption capacity, reflected in the Langmuir volume, is also inconclusive similar to sorption capacity at different pressures as discussed before, with only the CH_4 ultimate sorption capacity of the cryo-milled JH sample decreasing with all other experimental pairs increasing.

From a geological perspective, it is worthwhile mentioning that the JH coal mine is CO_2-dominated due to offgassing from an underlying magma intrusion, with the outburst incident reported near this site driven by CO_2. Consequently, the divergent trends observed in the ultimate sorption capacities for CH_4 and CO_2 in the cryomilled JH sample could be attributed to the preferential affinity to CO_2, greater than the effect of normal competitive adsorption between CO_2 and

CH_4. This may reverse the effects of cryom-illing observed in its CH_4 sorption. However, there is no direct evidence to support this theory so far. Therefore, the size information alone remains insufficient to accurately assess the sorption capacity of the coal. Nonetheless, an analysis of the experimental data reveals that the ratio of ultimate CH_4 sorption capacity between JH and KINGII, as well as the ratio for CO_2 before cryo-milling, is 1.34 and 1.38, respectively. After cryo-milling, these ratios diverge to 1.04 and 1.43, indicating that the ultimate sorption capacity to CO_2 is more responsive to changes in the JH particle size.

3.3 Gas diffusivity coefficients

3.3.1 Overall diffusivity coefficients

The overall diffusivity during the first 20 min was calculated from Eq. (16) and is depicted in Fig. 7. Both the 60–80 mesh and the further cryo-milled samples have been tested on both gasses with JH exhibiting higher effective diffusivity and with the distinction more significant in the case of the 60–80 mesh samples. This finding aligns with previous observations, which note that tectonically deformed coals such as JH exhibit higher diffusivity. This is attributed increased pore volume and specific surface area across micropores, mesopores, and macropores and enhanced pore connectivity (Wang et al. 2020; Guo et al. 2023a, b). This again highlights the importance of diffusivity on the outburst triggering as shown in Fig. 1.

After cryo-milling, the diffusivities of both samples increased with the JH sample retaining higher diffusivity. However, the KINGII diffusivities were more substantially increased during this process (Fig. 7). This may be attributed to grinding/milling/crushing altering the diffusion paths within the matrix, reducing flow resistance and opening pores that were previously dead-end pores, thus increasing diffusivity (Airey 1968; Bertard et al. 1970; Siemons et al. 2003b). However, the size effect only becomes apparent when the particle size is reduced to a certain range. Thus, it is inferred that cryo-milling introduces a size effect that increases the diffusivity. CH_4 increases with increasing pressure in all tests and this increase is larger than that for CO_2. This phenomenon is attributed to the increase in diffusion path length due to matrix swelling (Sander et al. 2020; Liwei et al. 2021). As pressure and gas content increase, swelling significantly reduces the roughness of the pore surfaces, resulting in a decrease in the diffusion path length—resulting in an increase in diffusivity. This reinforces why high gas pressure and high gas content are also necessary conditions for outbursts, stemming from their induced effects on diffusion properties.

3.3.2 Diffusivity coefficient decay with time (mass fraction method)

Equation (16) assumes that diffusivity is independent of time. This assumption is examined by varying the measurement time window in measuring a series of diffusivities under this local assumption. Results are illustrated in Fig. 8 and show that estimated diffusivitydecreases as the measurement time window is increased. This implies that the diffusivity calculated based on the entire experimental data represents an averaged value—with the initial diffusivity representative and the long term diffusivity overestimated.

Interestingly, variations in diffusivity were only observed at later times, indicating that no significant differences were

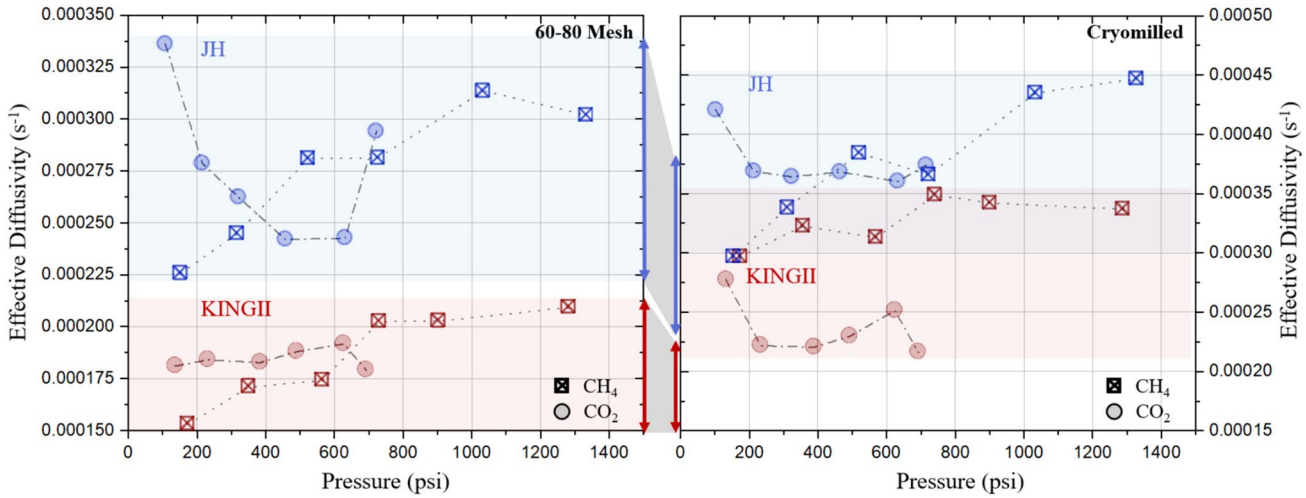

Fig. 7 Overall gas diffusivity (20 min) coefficient as a function of pressure

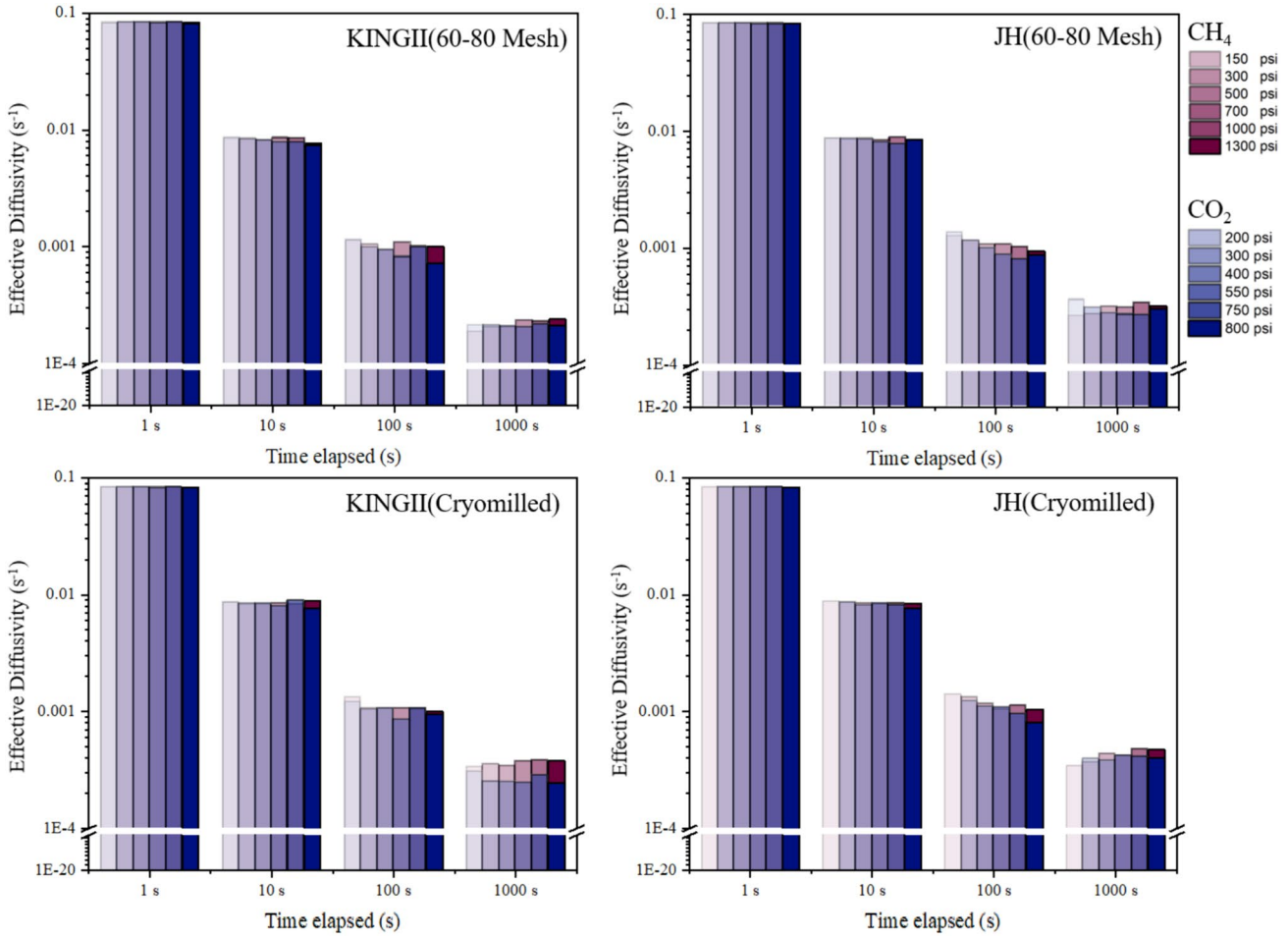

Fig. 8 Gas diffusivity coefficient in various time windows

evident during the early stages of the diffusion between samples and gasses. Between CO_2 and CH_4, CO_2 exhibits higher diffusivity as it is gas-type dependent for all coals. To gain a deeper insight into the decay of the diffusivity coefficient over time, as depicted in Fig. 9, diffusivity was calculated at each measured time. The results are aligned with Fig. 8. Furthermore, an overall power law relationship between diffusivity and time is apparent, especially at early times. The size and pressure effects remain the same as discussed in previous sections. Similar decay patterns have also been observed in previous studies involving dibromomethane and acetonitrile fluids in randomly packed spherical glass beads where this decay is associated with the geometrical properties of the pore systems (Li-wei et al. 2021). Another interesting observation from Fig. 9 is that the diffusivity tests involving CH_4 appear to be more sensitive to time compared to those with CO_2. This is evidenced by more divergent trends observed toward the end of the measurement period.

3.4 Time-resolved gas diffusion for early stage sorption

Time-resolved sorption dynamics are recovered from pressures captured at kHz resolution. The variations in sorption fraction over time for CH_4 sorption on KINGII are presented in Fig. 10 as representative of the results (data for CH_4 on JH and CH_4/CO_2 on KINGII are in the supplemental materials in Figure S-1, S-2, and S-3). For all the tests, clear linearity between sorption fraction and time was apparent within the first 10 s. The largest linear increasing trend was apparent for the cryomilled samples a their lowest pressure. Furthermore, all the tests conducted with cryomilled samples exhibited a higher sorption rate. Again, this observation is consistent with the observation that most coal outbursts occur in regions abundant with broken and small coal particles. A line representing this linearity was drawn on each of the figures. It apparent

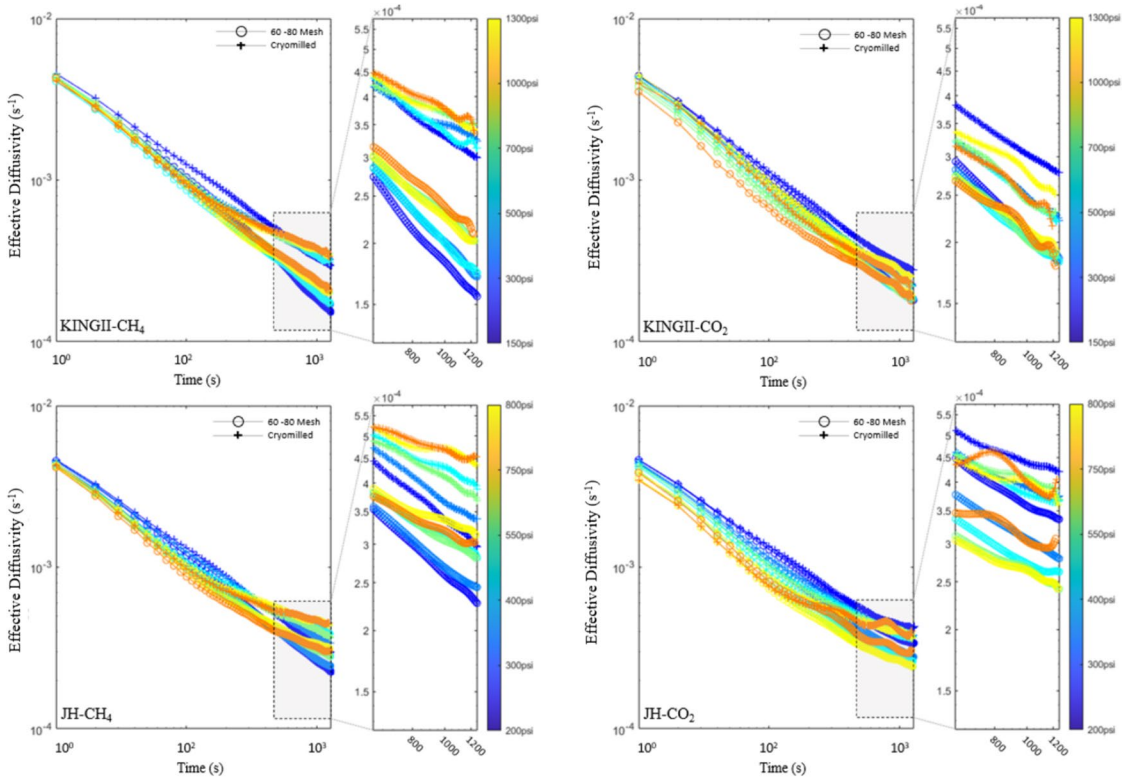

Fig. 9 Evolution of diffusivity with time

that with time elapsed, the sorption rate decreased and deviated from the linearity. This phenomenon is more pronounced in the cryomilled samples. Comparing across different samples and gasses, JH exhibited the steepest initial slope for both CH_4 and CO_2, highlighting its propensity for outbursts. It is important to note that this observed linearity deviates from the unipore model. This deviation arises since the assumption that the adsorbent particle is homogeneous and isotropic is violated. As depicted in Fig. 11a, the coal matrix is essentially neither homogeneous nor isotropic. This is attributed to its origin from stacked leaf-matter leaving pores arranged in a lamellar structure. Figure 11b shows an atomic force microscopy (AFM) image (Pan et al. 2015) of the macromolecular and pore structures of various coals with different ranks. This provides strong evidence that, at the matrix level, coal exhibits heterogonous and anisotropy properties. If pores are present, they provide a favorable path for mass transfer, differing from diffusion and resembling Darcian flow. In such a scenario, the slope of the transfer rate would be independent of time. When there are fractures and pores present, the apparent diffusion coefficient can be expressed as (Biloe et al. 2003):

$$D_a = D_e + \frac{k}{\mu_g} P \tag{17}$$

where D_a is the apparent diffusion coefficient, μ_g is the gas dynamic viscosity and k is the permeability. Relating to the linearity shown in Fig. 11a, diffusion mainly driven by mass transfer by time-independent pressure gradient dominates the early time rather than time-dependent effective diffusivity due to favorable paths. As time progresses and most of the favorable paths become gas filled, the coal matrix exhibits more homogeneous and isotropic gas transport characteristics, thus the diffusion is in turn mainly driven by time-dependent effective diffusivity. This observation further confirms that the use of an average overall diffusivity is an inaccurate and inadequate representation of the physics. This again aligns with the observation that outburst-prone coal typically exhibits highly developed pore structures, which contributes to the rapid release of gas at early time.

3.5 Kinetic sorption analysis

The initial linearity observed in the pressure–time response is a clear pattern of the zero-order kinetic adsorption model. Extensive kinetic analyses were carried out

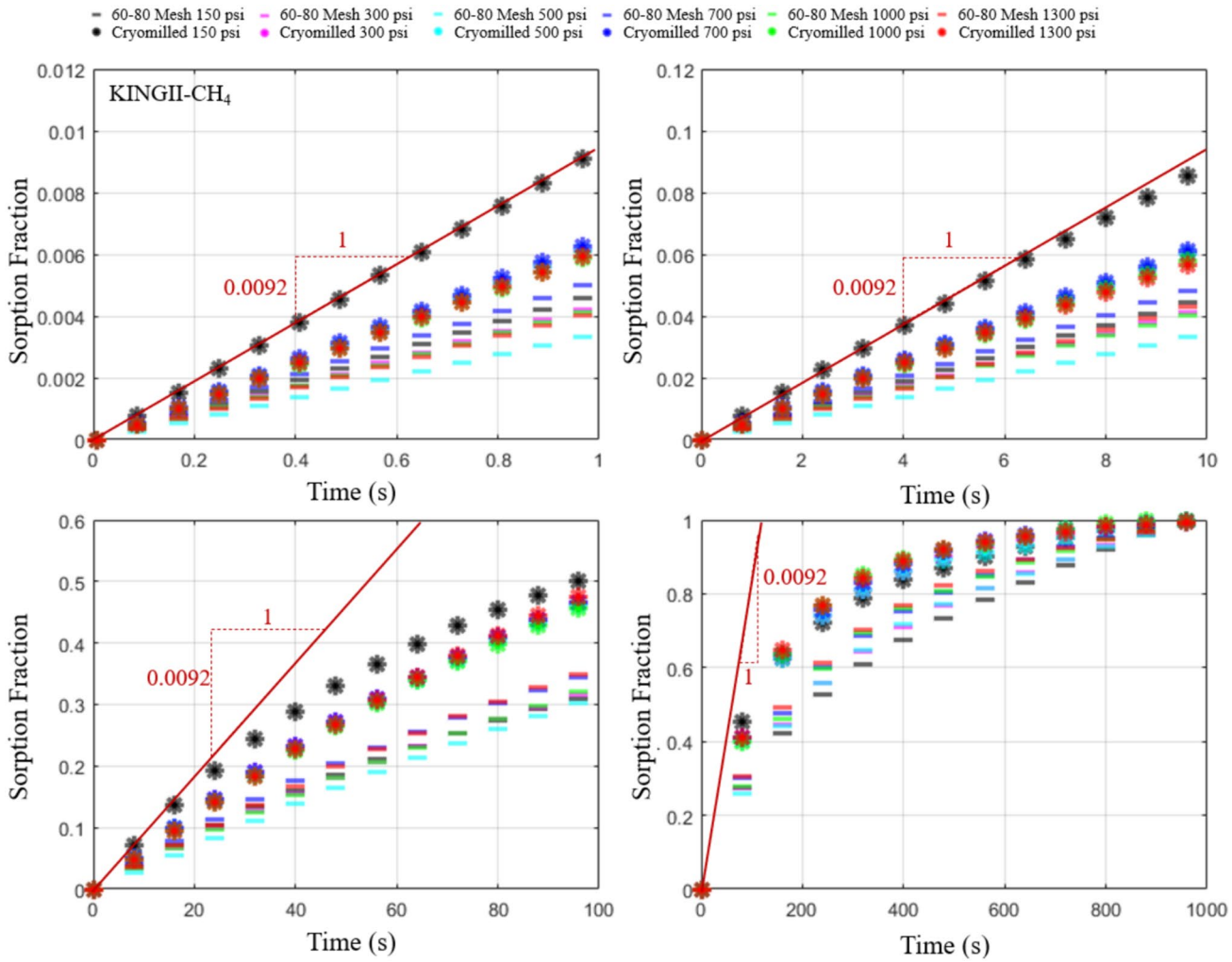

Fig. 10 Sorption fraction over different time capturing windows for CH_4 sorption on KINGII

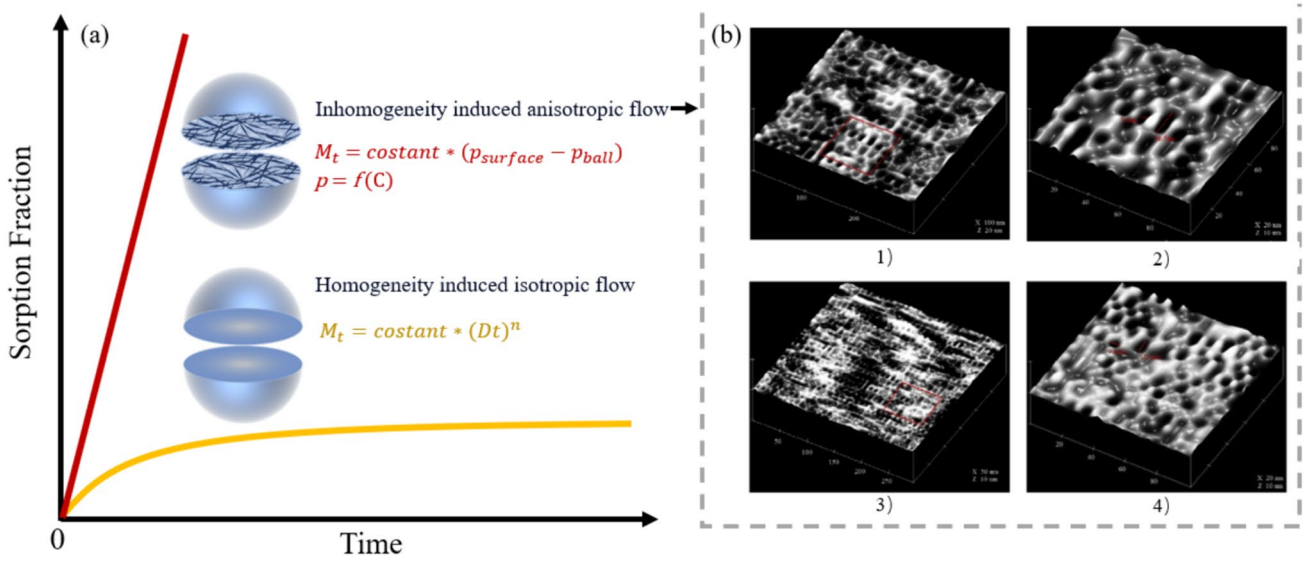

Fig. 11 **a** Illustration of anisotropic pore system-induced mass transfer flow; **b** AFM images for different weak brittle deformed coal samples: (1) Low-rank bituminous coal; (2) zoom-in of panel 1; (3) High-rank bituminous coal; (4) zoom-in of panel 3 (Pan et al. 2015).

Table 2 Kinetic equations to characterize dynamic sorption behavior

Model	Kinetic equations	Pattern
Zero order kinetic	$\frac{dM_t}{d} = k_0$	The adsorption rate k remains constant and is independent of the concentration. Thus, adsorption mass changes linearly with time
Pseudo first order	$M_t = M_\infty(1 - e^{-k_1 t})$	The adsorption rate k is relative to the gas concentration to be adsorbed. The pseudo first-order model is particularly apt for situations where there is a minimal change in the density of the adsorbed gas or when the alteration in the quantity of gas adsorbed is relatively small
Pseudo second order	$\frac{dM_t}{dt} = k_2(M_\infty - M_t)^2$	The adsorption rate k is relative to the gas concentration to be adsorbed. Additionally, the adsorption rate is steeper in the initial period before becoming constant at late time

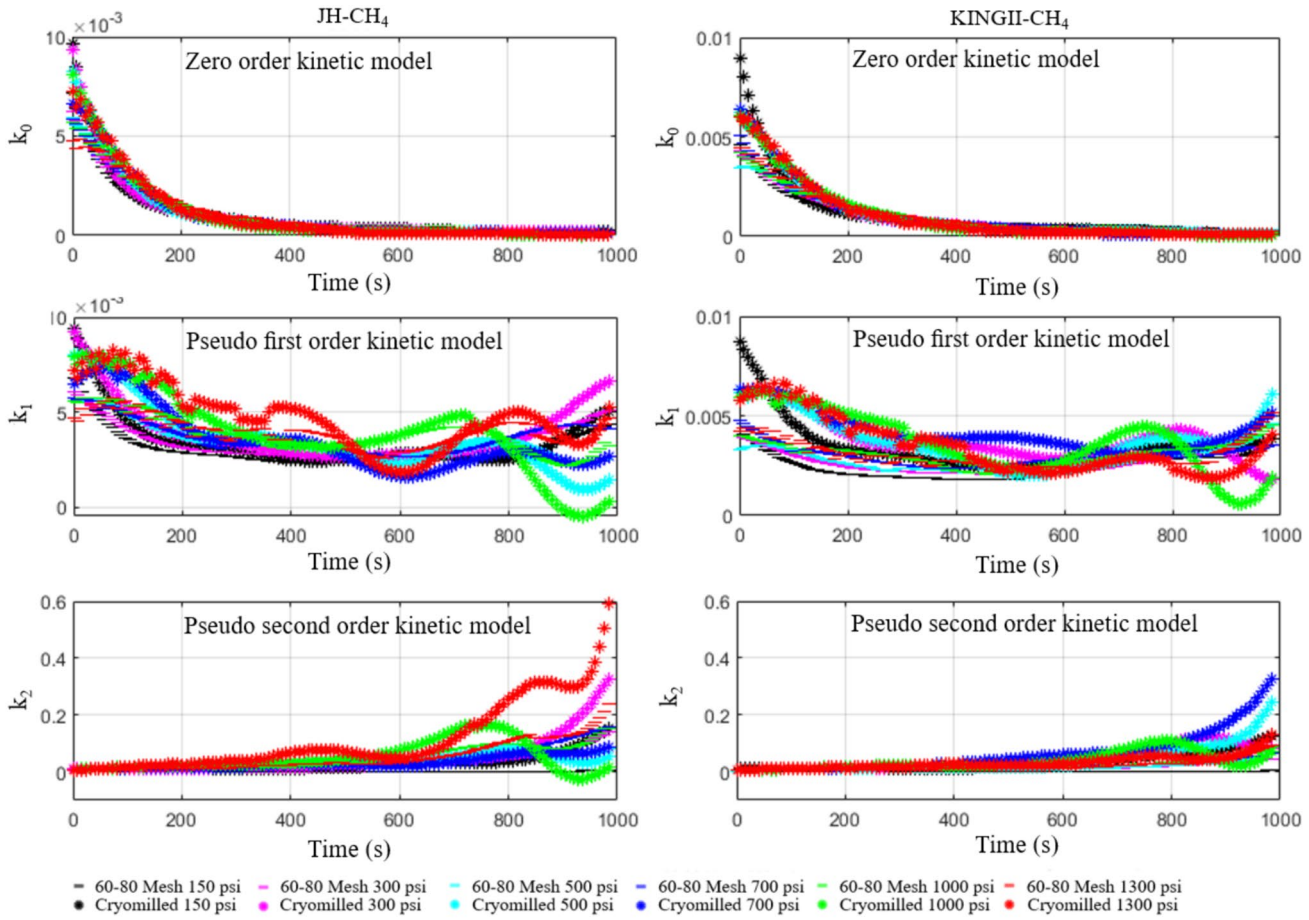

Fig. 12 Kinetic sorption characteristics for CH_4

using kinetic adsorption models using kinetic models initially developed to characterize chemical reaction processes—extensively used in chemical reaction-rate modeling. Due to their focus on surface reactions, akin to the dynamic equilibrium between free and adsorbed molecules during adsorption, these equations are also applicable for modeling surface sorption behavior. We summarize these kinetic models in Table 2

The modeling process was applied to all samples and gases and for the various models with the outcomes depicted in Figs. 12 and 13. Despite the linear trend over the first 10 s (Fig. 10), the zero-order kinetic adsorption rate declines rapidly in the initial stage. This suggests the disappearance of time-independent mass transfer at later times. In contrast, the pseudo –first-order kinetic adsorption rate shows considerable variability across all samples and gasses, especially when compared to the pseudo-second-order model. This variability reflects the failure of the model and indicates the presence of significant pressure decay in the early stages, violating the principal assumptions of the model. These findings confirm that rapid gas transfer predominantly occurs in the very initial stages

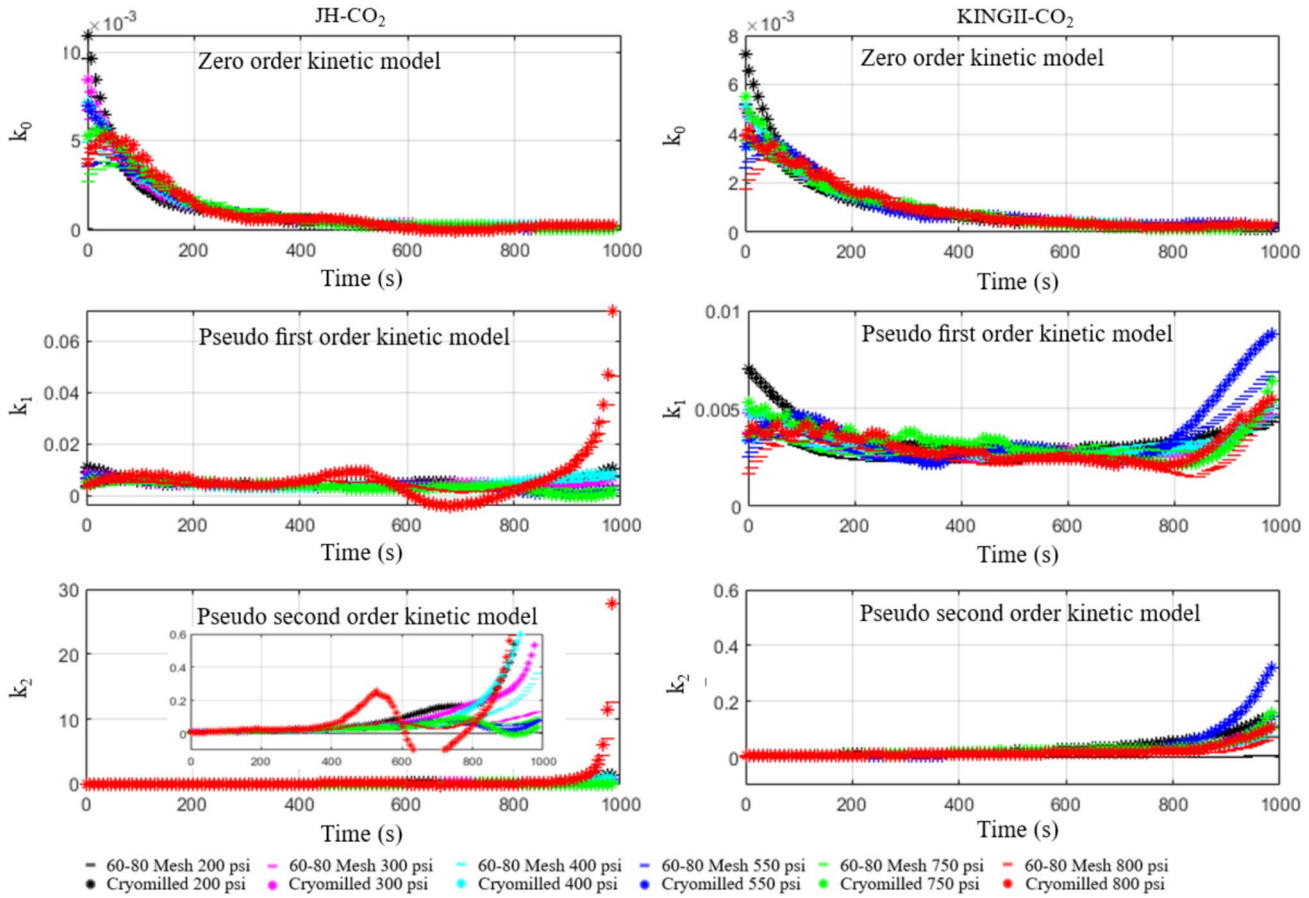

Fig. 13 Kinetic sorption characteristics for CO_2

of the process, as predicted by the pseudo-second-order model, which makes using an averaged overall diffusivity unreliable. Upon detailed examination of Fig. 13, it is observed that the pseudo-second-order adsorption rate for CO_2 sorption in JH is an order of magnitude greater than that in KINGII. Given the susceptibility of JH to CO_2 outbursts, this pseudo-second-order adsorption rate might potentially be used as an index for evaluating the risk of outbursts.

4 Conclusion

:: We have measured the sorption and diffusion characteristics of demonstrably outburst-prone and non-outburst-prone coals to understand their propensity for bursting. In particular, we have measured diffusion characteristics in the early stages of diffusion and fit these data to various kinetic diffusivity models. The main conclusions of this study are:

(1) Compared to non-outburst-prone coal (KINGII), the outburst-prone coal (JH) is readily pulverized, suggesting a low particle–particle strength. This suggests that JH coal is more susceptible to bursting during the outburst triggering stage and due to its low strength.
(2) Sorption capacities for both JH and KINGII coals are confirmed to be size-independent. However, sorption capacity is collectively influenced by the internal structural and external geometrical characteristics of the coal matrix.
(3) Cryomilling enhances diffusion in samples, with the CH_4-infiltrated coals showing a clear pressure-related increase. Diffusion in CO_2-infiltrated coals also increases with pressure due to matrix swelling altering diffusion paths.
(4) Temporal analyses using progressively larger time windows show decreasing diffusivity, challenging the reliability of average measures that ignore temporal variations. These variations are crucial for accurately predicting early-time diffusion characteristics, particularly in dynamic scenarios like gas outbursts.
(5) Early-stage gas diffusion studies show that initial mass transfer, driven by a steady pressure gradient, becomes time-dependent as the coal matrix changes. This under-

mines the accuracy of average diffusivity coefficients, especially in outburst-prone coals, emphasizing the need for understanding these dynamics to enhance safety in the coal industry.

(6) Kinetic sorption analyses reveal rapid gas transfer primarily in early phases, consistent with pseudo-second-order model predictions. This highlights the inadequacy of average diffusivity in capturing process dynamics. Additionally, the pseudo-second-order equation could help assess outburst risks in sensitive coals.

Supplementary Information The online version contains supplementary material available at https://doi.org/10.1007/s00603-024-03952-0.

Author contributions Xinxin He: Conceptualization, Methodology, Software, Investigation, Formal analysis, Writing—original draft, Visualization. Shimin Liu: Conceptualization, Methodology, Supervision, Resources, Funding acquisition, Writing—review & editing. Derek Elsworth: Supervision, Validation, Writing—review & editing.

Funding No external funding was used.

Declarations

Conflict of interest The authors declare that they have no known competing financial interests or personal relationships that could have appeared to influence the work reported in this paper.

References

Airey EM (1968) Gas emission from broken coal. An experimental and theoretical investigation. Pergamon Press

Arora NK, Mishra I (2019) United Nations Sustainable Development Goals 2030 and environmental sustainability: race against time. Environ Sustain 2:339–342. https://doi.org/10.1007/s42398-019-00092-y

ASTM International (2018) Standard practice for reducing samples of aggregate to testing size

Beamish BB, Crosdale PJ (1998) Instantaneous outbursts in underground coal mines: an overview and association with coal type

Bertard C, Bruyet B, Gunther J (1970) Determination of desorbable gas concentration of coal (DIRECT METHOD)* Summary of certain fundamental concepts concerning the gas-coal bond~1. Nature of Bond. Pergamon Press

Biloe S, Mauran S, Mauran M (2003) Gas flow through highly porous graphite matrices. Carbon 41:525–537

Busch A, Gensterblum Y, Krooss BM, Littke R (2004) Methane and carbon dioxide adsorption-diffusion experiments on coal: Upscaling and modeling. Int J Coal Geol 60:151–168. https://doi.org/10.1016/j.coal.2004.05.002

Cao J (2016) Statistical analysis of unsafe act reasons in coal and gas outburst accidents. Ind Saf Environ Prot 42:37

Cui X, Bustin RM, Dipple G (2004) Selective transport of CO2, CH4, and N2 in coals: Insights from modeling of experimental gas adsorption data. Fuel 83:293–303. https://doi.org/10.1016/j.fuel.2003.09.001

Ding Y, Cai W, Kong Y et al (2016) Signal characteristics of coal and rock dynamics with micro-seismic monitoring technique. Elsevier. https://doi.org/10.1016/j.ijmst.2016.05.022

Gray I (1987) Reservoir engineering in coal seams: part 1—the physical process of gas storage and movement in coal seams. SPE Reserv Eng 2:28–34. https://doi.org/10.2118/12514-PA

Guo H, Yu Y, Wang K et al (2023a) Kinetic characteristics of desorption and diffusion in raw coal and tectonic coal and their influence on coal and gas outburst. Fuel. https://doi.org/10.1016/j.fuel.2023.127883

Guo H, Yu Y, Wang Y et al (2023b) Experimental study on the desorption law and diffusion kinetic characteristics of gas in raw coal and tectonic coal. Energy. https://doi.org/10.1016/j.energy.2023.129924

Guo J, Kang T, Kang J et al (2014) Effect of the lump size on methane desorption from anthracite. J Nat Gas Sci Eng 20:337–346. https://doi.org/10.1016/j.jngse.2014.07.019

Hargraves A (1983) Prevention of instantaneous outbursts of coal and gas. Queensl Gov Min J (Australia) 84:

He X, Cheng Y, Hu B et al (2020) Effects of coal pore structure on methane-coal sorption hysteresis: an experimental investigation based on fractal analysis and hysteresis evaluation. Fuel 269:117438. https://doi.org/10.1016/j.fuel.2020.117438

Hou P, Su S, Gao F et al (2022) Influence of liquid nitrogen cooling state on mechanical properties and fracture characteristics of coal. Rock Mech Rock Eng 55:3817–3836. https://doi.org/10.1007/s00603-022-02851-6

Hou W, Wang H, Yuan L et al (2021) Experimental research into the effect of gas pressure, particle size and nozzle area on initial gas-release energy during gas desorption. Int J Min Sci Technol 31:253–263. https://doi.org/10.1016/J.IJMST.2021.01.002

Hu B, Cheng Y, He X et al (2020) New insights into the CH4 adsorption capacity of coal based on microscopic pore properties. Fuel. https://doi.org/10.1016/j.fuel.2019.116675

Huang L, Li B, Wang B et al (2023) Study on mechanical properties and energy evolution of coal under liquid nitrogen freezing. Eng Fract Mech. https://doi.org/10.1016/j.engfracmech.2023.109158

International Energy Agency (2023) Coal 2023 - Analysis and forecast to 2026

Hanes J, Lama RD, Shepherd J (1983) Research into the phenomenon of outbursts of coal and gas in some australian collieries. In: Paper presented at the 5th ISRM Congress, Melbourne, Australia, April 1983.

Jiang C, Chen S, Chen Y (1996) Measurement of the initial releasing energy of expanding methane from coal. Chin J Rock Mech Eng 15:359–400

Jin K, Cheng Y, Ren T et al (2018) Experimental investigation on the formation and transport mechanism of outburst coal-gas flow: Implications for the role of gas desorption in the development stage of outburst. Int J Coal Geol 194:45–58. https://doi.org/10.1016/j.coal.2018.05.012

Lama RD (1996) Outbursts of gas, coal and rock in underground coal mines

Lange C (1892) Outburst of carbon dioxide at the Rochbelle Mine. Bulletin Soc 1144–80

Linstrom PJ, Mallard WG (2001) The NIST chemistry WebBook: a chemical data resource on the Internet. J Chem Eng Data 46:1059–1063. https://doi.org/10.1021/JE000236I

Liu A, Liu P, Liu S (2020a) Gas diffusion coefficient estimation of coal: a dimensionless numerical method and its experimental validation. Int J Heat Mass Transf. https://doi.org/10.1016/j.ijheatmasstransfer.2020.120336

Liu A, Liu S, Hou X, Liu P (2020b) Transient gas diffusivity evaluation and modeling for methane and helium in coal. Int J Heat Mass Transf. https://doi.org/10.1016/j.ijheatmasstransfer.2020.120091

Li-wei C, Lin W, Tian-hong Y, Hong-min Y (2021) Deformation and swelling of coal induced from competitive adsorption of CH4/CO2/N2. Fuel. https://doi.org/10.1016/j.fuel.2020.119356

Lowell S, Shields J, Thomas M, Thommes M (2006) Characterization of porous solids and powders: surface area, pore size and density

Mavor MJ, Pratt TJ (1990) Measurement and evaluation of coal sorption isotherm data

Meng Y, Tang D, Xu H et al (2014) Division of coalbed methane desorption stages and its significance. Pet Explor Dev 41:671–677. https://doi.org/10.1016/S1876-3804(14)60080-X

Moore TA (2012) Coalbed methane: a review. Int J Coal Geol 101:36–81. https://doi.org/10.1016/j.coal.2012.05.011

Nandi SP, Walker PL (1969) Activated diffusion of methane in coal. Fuel 49:309–323

Nie W, Liu Y, Li CJ, et al (2014) A gas monitoring and control system in a coal and gas outburst laboratory. J Sens 2014:1–11

Nikolai Siemons, Andreas Busch, Hans Bruining, et al (2003a) Assessing the Kinetics and Capacity of Gas Adsorption in Coals by a Combined Adsorption/ Diffusion Method. In: Paper presented at the SPE Annual Technical Conference and Exhibition, Denver, Colorado

Nikolai Siemons, Andreas Busch, Hans Bruining, et al (2003b) Assessing the Kinetics and Capacity of Gas Adsorption in Coals by a Combined Adsorption/ Diffusion Method. In: SPE Annual Technical Conference and Exhibition. Denver, Colorado

Pan J, Zhu H, Hou Q et al (2015) Macromolecular and pore structures of Chinese tectonically deformed coal studied by atomic force microscopy. Fuel 139:94–101. https://doi.org/10.1016/j.fuel.2014.08.039

Paterson L (1986) A model for outbursts in coal. Int J Rock Mech Min Sci 23:327–332. https://doi.org/10.1016/0148-9062(86)90644-3

Qin L, Ma C, Li S et al (2022) Mechanical damage mechanism of frozen coal subjected to liquid nitrogen freezing. Fuel. https://doi.org/10.1016/j.fuel.2021.122124

Qixiang Y (1990) Study on the threshold gas pressure in coal and gas outburst. Journal of China University of Mining and Technology

Rouquerol J, Rouquerol F, Llewellyn P, Maurin G (2013) Adsorption by powders and porous solids: principles, methodology and applications

Ruppel TC, Grein CT, Bienstock D (1974) Adsorption of methane on dry coal at elevated pressure

Sander R, Connell LD, Camilleri M, Pan Z (2020) CH4, CO2, N2 diffusion in Bowen Basin (Australia) coal: relationship between sorption kinetics of coal core and crushed coal particles. J Nat Gas Sci Eng. https://doi.org/10.1016/j.jngse.2020.103468

Sato K, Fujii Y (1989) Source mechanism of a large scale gas outburst at Sunagawa Coal Mine in Japan. PAGEOPH 129:325–343. https://doi.org/10.1007/BF00874513

Si G, Durucan S, Jamnikar S et al (2015) Seismic monitoring and analysis of excessive gas emissions in heterogeneous coal seams. Elsevier

Tu Q, Cheng Y, Xue S et al (2021) Energy-limiting factor for coal and gas outburst occurrence in intact coal seam. Int J Min Sci Technol 31:729–742. https://doi.org/10.1016/j.ijmst.2021.05.009

United Nations (2015) Transforming our world: the 2030 agenda for sustainable development

Valliappan S, Wohua Z (1999) Role of gas energy during coal outbursts. Int J Numer Methods Eng 44:875–895

Wang F, Zhang P, Cui B et al (2021) Research progress of disaster factors and a prevention alarm index of coal and gas outbursts. Arab J Geosci. https://doi.org/10.1007/S12517-021-07540-2

Wang H, Zhang Y, Yuan L et al (2019) Analysis of influence law and temperature effect of initial released gas expansion energy of the coal grain. J Min Saf Eng 36:1052–1060. https://doi.org/10.13545/j.cnki.jmse.2019.05.024

Wang X, Zhang D, Su E et al (2020) Pore structure and diffusion characteristics of intact and tectonic coals: Implications for selection of CO2 geological sequestration site. J Nat Gas Sci Eng. https://doi.org/10.1016/j.jngse.2020.103388

Yang Y (2020) Modeling of gas sorption and diffusion behavior and implications on coalbed methane production a. Dissertation in Energy and Mineral Engineering

Yang Y, Liu S (2020a) Laboratory study of cryogenic treatment induced pore-scale structural alterations of Illinois coal and their implications on gas sorption and diffusion behaviors. J Pet Sci Eng. https://doi.org/10.1016/j.petrol.2020.107507

Yang Y, Liu S (2021) Integrated modeling of multi-scale transport in coal and its application for coalbed methane recovery. Fuel. https://doi.org/10.1016/j.fuel.2021.120971

Yang Y, Liu S (2019) Estimation and modeling of pressure-dependent gas diffusion coefficient for coal: a fractal theory-based approach. Fuel 253:588–606. https://doi.org/10.1016/j.fuel.2019.05.009

Yang Y, Liu S (2020b) Review of shale gas sorption and its models. Energy Fuels 34:15502–15524

Yang Y, Liu S, Clarkson C (2022) Quantification of temperature-dependent sorption isotherms in shale gas reservoirs: experiment and theory

Yang Yu (2019) Micropore volume modification for coal using non-contaminating cryogenic liquid nitrogen and its impact on sorption and diffusion behaviors

Zhang X, Tang J, Yu H, et al (2022) Gas pressure evolution characteristics of deep true triaxial coal and gas outburst based on acoustic emission monitoring. Sci Rep 12:21738

Zhao W, Wang K, Wang L et al (2021) Influence of matrix size and pore damage path on the size dependence gas adsorption capacity of coal. Fuel. https://doi.org/10.1016/j.fuel.2020.119289

Li Z, Zhao B (2012) Microseism monitoring system for coal and gas outburst. Int J Comp Sci Issues 9